ACS APPLIED ELECTRONIC MATERIALS

pubs.acs.org/acsaelm

Article

Local Environment of Sc and Y Dopant Ions in Aluminum Nitride Thin Films

Asaf Cohen, Junying Li, Hagai Cohen, Ifat Kaplan-Ashiri, Sergey Khodorov, Ellen J. Wachtel, Igor Lubomirsky,* Anatoly I. Frenkel,* and David Ehre*

Cite This: *ACS Appl. Electron. Mater.* 2024, 6, 853−861

Read Online

ACCESS | Metrics & More | Article Recommendations | Supporting Information

ABSTRACT: The local environments of Sc and Y in predominantly ⟨002⟩ textured, $Al_{1-x}Do_xN$ (Do = Sc, x = 0.25, 0.30 or Y, x = 0.25) sputtered thin films with wurtzite symmetry were investigated using X-ray absorption (XAS) and photoelectron (XPS) spectroscopies. We present evidence from the X-ray absorption fine structure (XAFS) spectra that, when x = 0.25, both Sc^{3+} and Y^{3+} ions are able to substitute for Al^{3+}, thereby acquiring four tetrahedrally coordinated nitrogen ligands, i.e., coordination number (CN) of 4. On this basis, the crystal radius of the dopant species in the wurtzite lattice, not available heretofore, could be calculated. By modeling the scandium local environment, extended XAFS (EXAFS) analysis suggests that when x increases from 0.25 to 0.30, CN for a fraction of the Sc ions increases from 4 to 6, signaling octahedral coordination. This change occurs at a dopant concentration significantly lower than the reported maximum concentration of Sc (42 mol % Sc) in wurtzite (Al, Sc)N. XPS spectra provide support for our observation that the local environment of Sc in (Al, Sc)N may include more than one type of coordination.

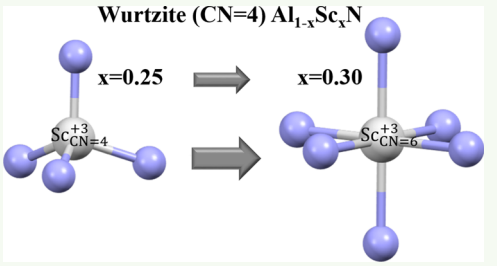

KEYWORDS: *aluminum scandium nitride, aluminum yttrium nitride, sputtering, seeding layer, texture, piezoelectric*

INTRODUCTION

During the search for lead-free, Si-microfabrication compatible piezoelectric materials, thin films of doped aluminum nitride (AlN) have stimulated considerable interest. As actuators,[1] energy harvesters[2] and as components of microelectromechanical-systems (MEMS),[3] they show promising results. Among the reasons for applications of AlN in MEMS devices are its high-temperature stability, high Curie temperature (T_c = 1423 K), and low relative dielectric permittivity (∼10).[3] However, the piezoelectric constants of AlN thin films are relatively low compared to those of other piezoelectric materials, and metal doping has been shown to be beneficial in this regard. Among the dopants used to increase the material piezoelectric coefficients are codopants magnesium/niobium,[4] trivalent scandium[5,6] and the less costly, trivalent yttrium.[3] Notably, *c*-axis-tilted (Al, Y)N thin films display high shear electromechanical coupling constants, which makes them very promising, high-performance materials for surface acoustic wave (SAW) and bulk acoustic wave (BAW) detection.[7]

However, preparation of (Al, Sc)N films is challenging because ScN and YN (both rock-salt-type ($Fm\bar{3}m$) symmetry, space group #225) and AlN (wurtzite-type $P6_3m$, polar space group #176) are totally immiscible.[8] As a result, substitutional solid solutions of AlN with ScN or YN are thermodynamically unstable under ambient conditions and undergo phase segregation. This instability has been attributed, at least in part, to the considerable disparity in crystal radius between aluminum (67.5 pm) and scandium or yttrium (88.5 or 104 pm, respectively), for coordination number (CN) 6.[9] Lowering CN to 4, would be expected to further reduce the crystal radius for all three elements, although a value has been determined only for Al (53 pm). Consequently, successful deposition of the metastable phases of AlDoN (Do = Sc or Y), with controlled *c*-axis orientation, a desirable property for piezoelectric applications, presents a significant challenge. Reactive sputtering allows synthesizing solid solutions away from thermodynamic equilibrium, so even metastable phases can be obtained, in spite of the internal driving force toward phase separation into domains with different crystal structures. Additional deposition parameters which must be optimized include: temperature,[6] deposition pressure,[10] seed-layer epitaxy,[11] and substrate surface roughness.[12]

While incorporation of these dopants into the AlN wurtzite phase has been demonstrated by X-ray diffraction (XRD), i.e., progressive increase in the lattice parameters and in the piezoelectric response,[6,13,14] little is known concerning the local environment of the dopant. Akiyama et al. demonstrated incorporation of the Sc^{3+} ion into the wurtzite phase at mole fraction ≤42%, beyond which phase separation occurs, even

Received: October 5, 2023
Revised: January 4, 2024
Accepted: January 4, 2024
Published: January 19, 2024

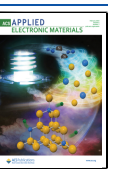

upon sputtering.[6,13] This study also found that, as the concentration of Sc increased to 27 mol %, the 002 diffraction peak of the wurtzite phase moved to lower diffraction angles, i.e., the *c*-axis periodicity increased. However, beyond 27 mol %, the 002-peak moved to higher diffraction angles. The significance of the concentration at which this reversal occurred has not been addressed. The authors suggested that development of local stress/strain during the deposition process might have contributed to phase segregation of ScN. Incorporation of Y into the AlN wurtzite phase is even more restrictive.[15]

The present work investigates the effective size and local environment of trivalent Sc and Y ions within the host AlN wurtzite lattice. Extended X-ray absorption fine structure (EXAFS) spectroscopy and X-ray photoelectron spectroscopy (XPS) measurements provide evidence that, for both Sc and Y, the majority of the dopant ions, upon substitution for an aluminum ion, acquire four N atoms as near neighbors. For the case of Sc, we also observed that, at 30 mol % doping, a minor fraction of the ions are coordinated by 6, rather than 4, nitrogen ions. We were able to discount the possibility of Sc^{3+} coordinated by 5 nitrogen ions. There are no literature reports of binary compounds of 5-coordinated Sc. A successful attempt to stabilize 5-coordinated, trivalent Sc, involving multicomponent (including P, N, Cl, O, and Si) organometallic synthesis, has in fact been described.[16] However, that possibility is not relevant to the structures investigated here. Consequently, we proposed either a homogeneous model (all Sc atoms are in a 4-coordinated state) or a heterogeneous model (Sc atoms partition between 4 and 6-coordinated states). The second model is the more probable for $Al_{0.70}Sc_{0.30}N$.

These findings support the concept that the phase separation observed at 42 mol % Sc must, in fact, be the culmination of a gradual process. Additionally, by calculating the number of nearest neighbors and bond lengths obtained from XAS measurements, we are able to report estimates of the effective size of $Sc^{3+}_{CN=4}$ and $Y^{3+}_{CN=4}$ in the wurtzite lattice.

EXPERIMENTAL SECTION

Materials. N_2, argon, and O_2 sputtering gases (Gas Technologies, Israel, 99.9999 purity) were used. Hydrofluoric acid (HF), organic solvents, acetone, and isopropyl alcohol (IPA) were semiconductor CMOS grade (Sigma-Aldrich). Scandium nitride (ScN) powder (99.9% purity, Sigma-Aldrich) was used for EXAFS measurements.

Deposition of $Al_{1-x}Do_xN$ (Do = Sc, x = 0.25, 0.30 or Y, x = 0.25) Thin Films. $(Al_{1-x}Do_x)N$ (Do = Sc, x = 0.25, 0.30 or Y, x = 0.25) films were deposited by direct current (DC) reactive sputtering onto Ti seeding layers. The conditions under which the Ti layers were deposited are described in detail in Cohen et al.[17] Two-inch diameter substrates were used: ⟨100⟩ cut \p-type Si wafers, resistivity 10−30 Ω·cm, University Wafers, thickness 250 ± 25 μm. The substrates were cleaned with solvents in order of increasing polarity: acetone, isopropyl alcohol, deionized water. Dilute (4 vol %) HF was then used to remove the native oxide layer as well as surface contaminants. The substrates underwent argon and oxygen plasma cleaning to remove organic contaminants in the sputtering chamber at 10 mTorr pressure with oxygen/argon volume ratio of 1:1. Pressure in the chamber was lowered to 5 mTorr with volume ratio between argon and nitrogen 1:4. Without breaking the vacuum following deposition of the Ti seeding layers, the substrates were heated in the sputtering chamber to 673 ± 10 K. 250 W power was then applied to a 3 in. diameter magnetron loaded with a 5N purity metal alloy target $(Al_{1-x}Sc_x)$ (x = 0.25, 0.30), or 3N purity metal alloy target $Al_{0.75}Y_{0.25}$ (all from Abletargets, China). Reactive DC sputtering from the metallic alloy target, $Al_{1-x}Do_x$, was performed for 30 min in nitrogen/argon plasma. Deposition at a rate of 3.5−4 nm/min was then continued at 523 K for 8 h to achieve the desired film thickness (2 μm).

Film Characterization. Film thickness was measured on sample cross sections imaged with a scanning electron microscope (SEM, Zeiss Sigma 500, and Zeiss Supra 55VP, 4−8 keV). SEM images were also used to estimate the mean grain size and morphology of both the surface and cross-section. Elemental analysis was performed by energy dispersive X-ray spectroscopy (EDS) using a four-quadrant detector (Bruker, FlatQUAD) installed on the Zeiss Ultra 55 SEM. Accelerating voltage was 20 kV. X-ray diffraction (XRD) patterns were collected with a TTRAX III diffractometer (Rigaku, Japan) in the Bragg−Brentano mode. Voigt profile fitting was applied to the 002 diffraction peaks (Jade, MDI). The intensity and line width of the $(Al_{1-x}Do\ x)N$ (Do = $Sc_{x=0.25,0.30}$ or $Y_{x=0.25}$), 002 diffraction peak monitored the extent of *c*-axis texture and crystallinity perpendicular to the plane of the substrate. Film in-plane stress (σ) was deduced from the change in the wafer curvature, before and after film deposition, using a DektakXT stylus profilometer. The Stoney formula was used for calculation of residual in-plane film stress.[18] $\sigma = \frac{E_s h_s^2}{6(1-\nu_s)h_f}\left(\frac{1}{R} - \frac{1}{R_0}\right)$, where E is the Young's modulus; h is the thickness; ν is the Poisson's ratio; R is the cantilever radius of curvature following deposition; and R_0 is the initial radius of curvature. Subscripts s and f refer to the substrate and thin film, respectively. Since the doped AlN film was by far the thickest in the stack, in-plane stress was calculated neglecting the mechanical properties of other layers.

X-ray Photoelectron Spectroscopy (XPS). X-ray photoelectron spectroscopy (XPS, Kratos AXIS-Ultra DLD spectrometer with monochromatic Al Kα source, 15−75 W) was used for surface (8−10 nm) chemical analysis of the $Al_{1-x}Sc_xN$ layers, x = 0.25, 0.3 with ScN powder as a reference sample. In an attempt to eliminate beam-induced charging artifacts, the energy scale was referenced to the theoretical binding energy of N 1s in AlN. This somewhat arbitrary choice was cross-checked using a dedicated experimental procedure in which the total surface charging can be evaluated at any given time and referred to the zero-exposure limit. Thus, consistency between samples was kept high and the evaluation of fine changes in Sc binding energies approached accuracy ±<50 meV. Ar-ion sputtering at 4 keV beam energy was used, starting with short sputtering steps (~1 μA, on a 5 × 5 mm^2 raster for 30 s) and increasing gradually, in order to capture fine surface details and to identify potential beam-induced effects. In general, the layers exhibited robust behavior under the stepwise sputtering such that no metallic clusters were formed. Yet, Sc-oxide dilution upon increased sputtering time should be taken into account.

X-ray Absorption Spectroscopy. To study the oxidation state and near neighbor environment of Sc and Y dopants in thin films of $Al_{1-x}Sc_xN$ and $Al_{1-x}Y_xN$, X-ray absorption spectra (XAS) were collected at beamlines 8-BM (for Sc K-edge) and 7-BM (for Y K-edge) of the National Synchrotron Light Source (NSLS-II) at Brookhaven National Laboratory, New York. Thin film data were collected in fluorescence mode, whereas transmission mode was used for the yttrium foil. ScN and yttria powders were measured in the fluorescence mode (Table 1). EXAFS analysis was performed using the Demeter package to derive quantitative structural information concerning the near neighbor environment of Sc and Y in AlScN or AlYN.

RESULTS AND DISCUSSION

XRD, SEM, and EDS Characterization of Thin Films of $Al_{1-x}Do_xN$ (Do = Sc, x = 0.25, 0.30 or Y, x = 0.25). XRD patterns of AlScN films were dominated by a strong wurtzite 002 diffraction peak at 2θ = 35.73° for $Al_{0.75}Sc_{0.25}N$ (Figure 1) and at 2θ = 35.58° for $Al_{0.70}Sc_{0.30}N$ (Figure 1). In the case of $Al_{0.75}Y_{0.25}N$, three peaks were observed at 2θ = 31.31, 34.64 and 37.7° (Figure 2 and Supporting Section S1), which could

https://doi.org/10.1021/acsaelm.3c01390
ACS Appl. Electron. Mater. 2024, 6, 853−861

Table 1. Thin Film, Foil, and Powder Samples Examined by XAS

samples	edge	measurement mode
$Al_{0.75}Sc_{0.25}N$, $Al_{0.70}Sc_{0.30}N$	Sc K-edge	fluorescence
ScN powder	Sc K-edge	fluorescence
Y_2O_3 powder	Y K-edge	fluorescence
$Al_{0.75}Y_{0.25}N$	Y K-edge	fluorescence
Y foil	Y K-edge	transmission

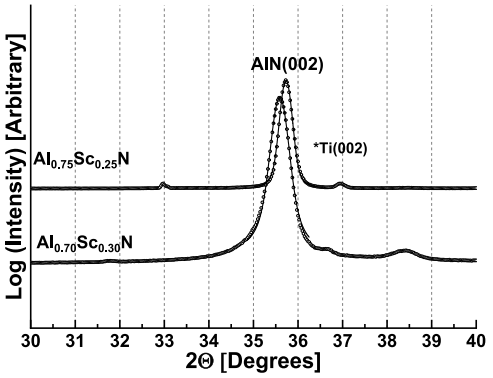

Figure 1. XRD patterns of $Al_{0.75}Sc_{0.25}N$ and $Al_{0.70}Sc_{0.30}N$ thin films grown on ⟨100⟩ cut Si wafers with a 50 nm Ti seeding layer. The substrate is tilted 3° in order to minimize diffraction from the Si substrate.

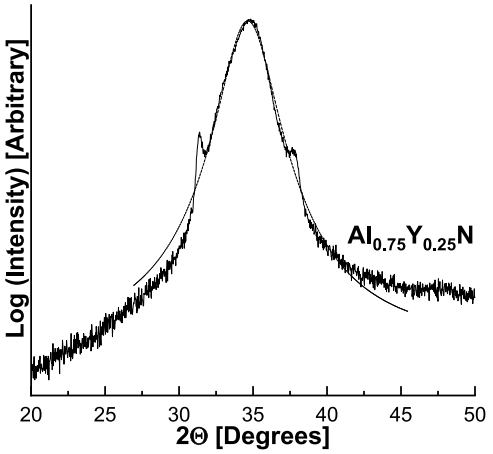

Figure 2. XRD pattern of an $Al_{0.75}Y_{0.25}N$ thin film grown on ⟨100⟩ cut Si with a 50 nm Ti seeding layer. A pattern with full 2θ range is included in the SI (Figure S1). The substrate has been tilted 3° in order to minimize diffraction from the Si substrate.

be indexed as being due to the (100), (002), (101) planes of the $P6_3m$ lattice, c = 5.11 Å, $a = b$ = 3.29 Å, γ = 120°. The minimum crystal size perpendicular to the plane of the substrate, calculated by the Scherrer formula from the full width at half height of the 002 diffraction peak, was 57 and 38 nm for $Al_{0.75}Sc_{0.25}$ and $Al_{0.70}Sc_{0.30}N$, respectively. The comparable value was 2.5 nm for the $Al_{0.75}Y_{0.25}N$ film. Scanning electron microscopy (SEM) imaging of the (AlSc)N films surface and cross-section (Figure 3a,b) shows pebble-like grains of mean transverse size of 84−92 nm, with columnar growth. In the case of $Al_{0.70}Sc_{0.30}N$, disoriented, pyramid-shaped grains occupy a minor fraction of the surface area. Although metal stoichiometry of the deposited films may differ from that of the alloy target, EDS showed negligible

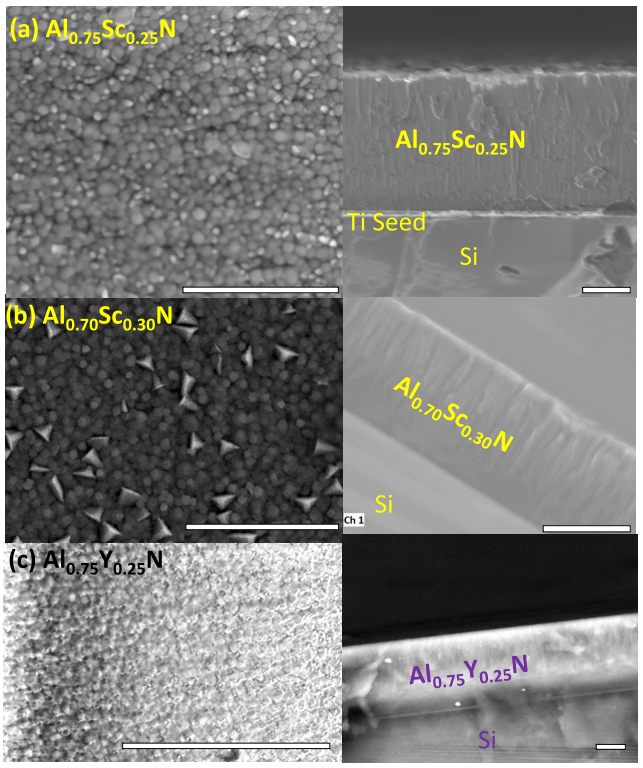

Figure 3. SEM images of the surface and cross-section of thin films (a diamond pen was used to prepare cross sections) of (a) $Al_{0.75}Sc_{0.25}N$, reproduced with permission from ref 17. (b) $Al_{0.70}Sc_{0.30}N$ and (c) $Al_{0.75}Y_{0.25}N$, respectively. Pebble-like grains (84−94 nm) appear on the surface in panels (a) and (b), along with columnar growth. Grain size decreases with increasing Sc concentration. Disoriented, abnormal grains are observed on the surface of $Al_{0.70}Sc_{0.30}N$. We noted in our earlier report[17] that during reactive sputtering of AlScN, the final deposition temperature influences the number of abnormally oriented grains visible in SEM images. In panel (c), individual grains and grain size on the film surface are difficult to distinguish, indicating a tendency to poor crystallinity, as has been reported in the literature.[15] All scale bars indicate 1 μm.

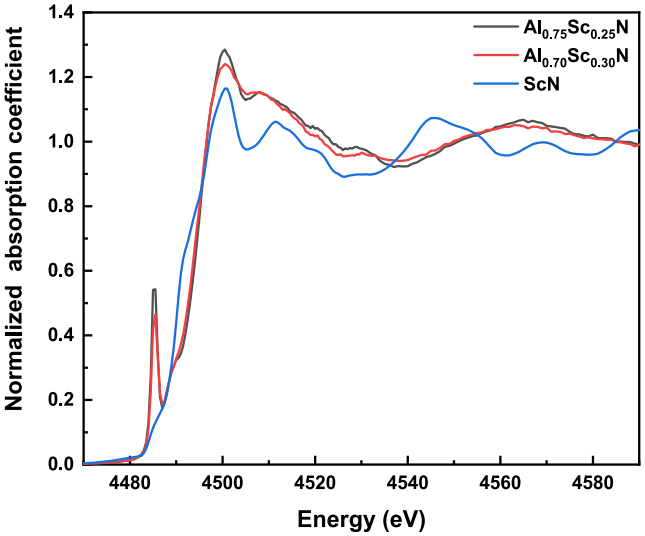

Figure 4. Sc K-edge XANES spectra of $Al_{0.75}Sc_{0.25}N$ (black trace), $Al_{0.7}Sc_{0.3}N$ (red trace) thin films, and ScN (blue trace) powder. Note the absence of a pre-edge peak for ScN.

https://doi.org/10.1021/acsaelm.3c01390
ACS Appl. Electron. Mater. 2024, 6, 853−861

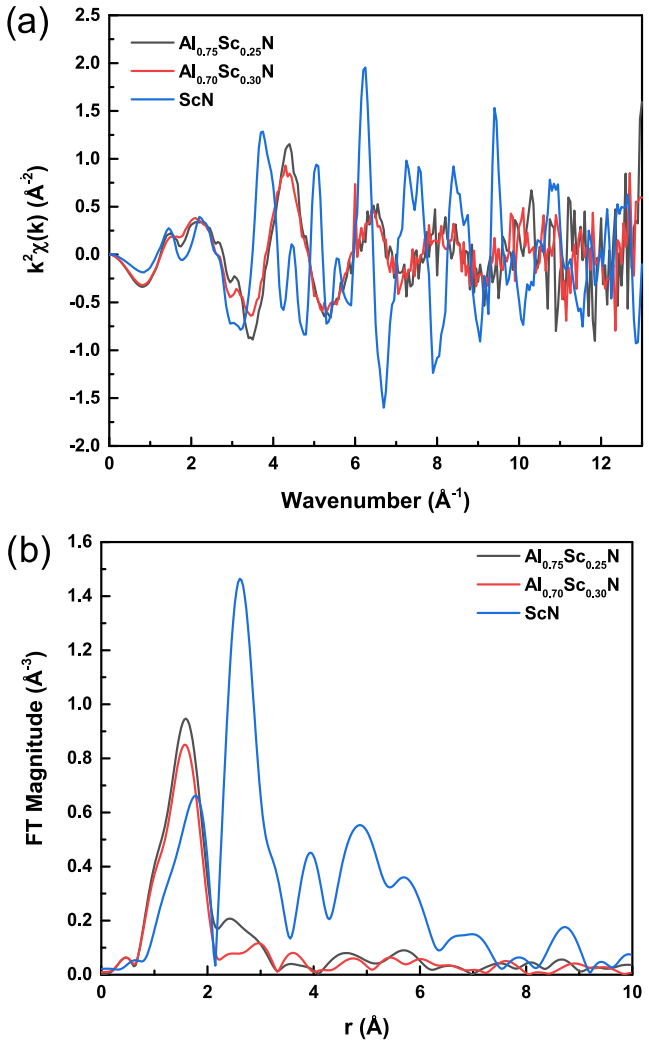

Figure 5. (a) k^2-weighted EXAFS spectra of $Al_{0.75}Sc_{0.25}N$ (black trace) and $Al_{0.7}Sc_{0.3}N$ (red trace) films and ScN (blue trace) powder; (b) Fourier transform magnitude of the k^2-weighted EXAFS spectra shown in panel (a). The k-range used for the Fourier transform was 2−9 Å^{-1}.

change, i.e., $Al_{0.75}Sc_{0.25}$, $Al_{0.70}Sc_{0.30}$, and $Al_{0.75}Y_{0.25}$ (see also Supporting Section S2). In-plane compressive stress of the films was 60 and 200 MPa for $Al_{0.75}Sc_{0.25}N$ and $Al_{0.70}Sc_{0.30}N$, respectively, and 1400 MPa for $Al_{0.75}Y_{0.25}N$ films, as calculated from the change in Si wafer curvature, using the Stoney formula.[18] Transverse grain size could not be determined for $Al_{0.75}Y_{0.25}N$ thin films due to excessive charging in the electron microscope.

X-ray Absorption Fine Structure (XAFS) of Sc-Doped Aluminum Nitride. The near neighbor environments of Sc^{3+} dopants were examined by Sc K-edge X-ray absorption spectroscopy (XAS). Both EXAFS and XANES measurements were analyzed. The presence of the pre-edge peak, denoted A, in the XANES spectra (Figure 4) of both $Al_{0.75}Sc_{0.25}N$ and $Al_{0.70}Sc_{0.30}N$, points to an asymmetric environment, i.e., the Sc^{3+} ion is not located at an inversion center.[19−22] This asymmetry would be expected for the tetrahedrally coordinated (CN = 4) scandium ion. By contrast, the pre-edge peak is absent in the XANES spectrum of ScN, which is consistent with the octahedrally coordinated environment (CN = 6) of the scandium ion in the rock-salt ($Fm\bar{3}m$) lattice. The pre-edge

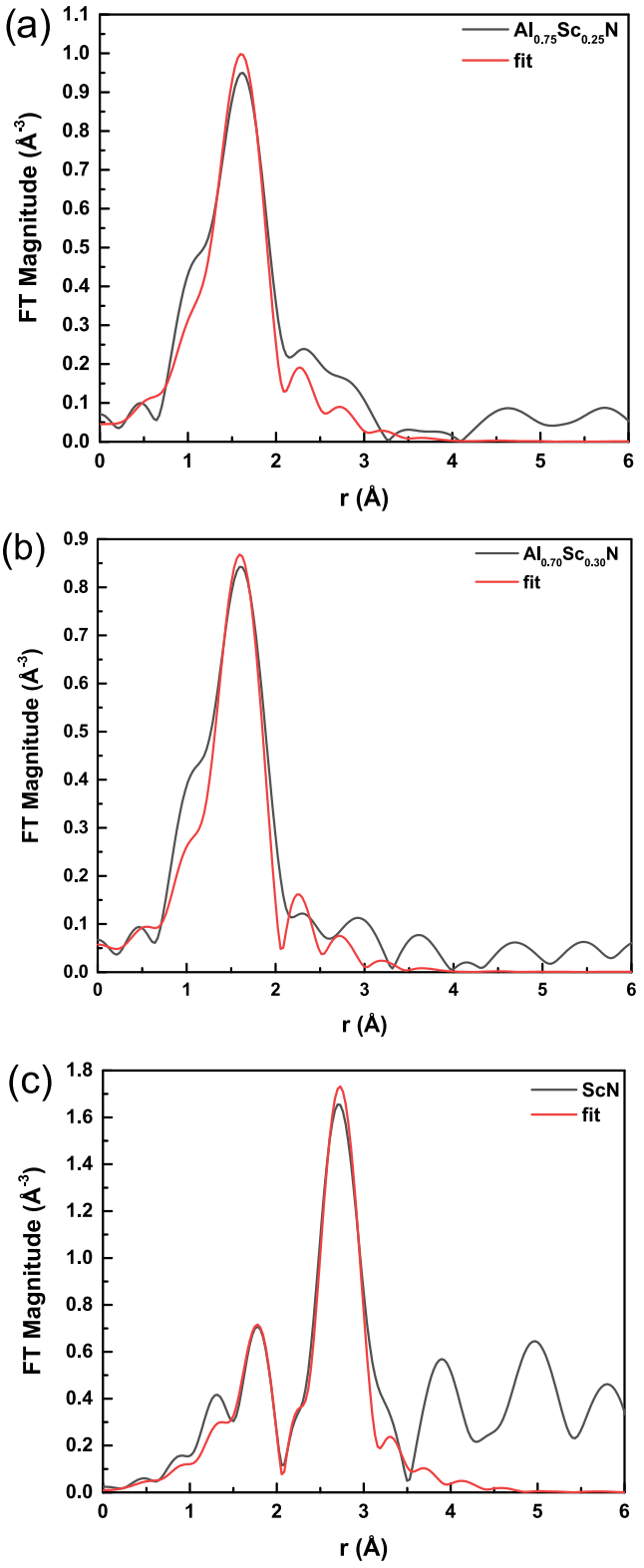

Figure 6. Fourier transform magnitude of k^2-weighted EXAFS spectra of (a) $Al_{0.75}Sc_{0.25}N$; (b) $Al_{0.7}Sc_{0.3}N$; (c) ScN, accompanied by theoretical fits. Best fit parameters are tabulated in Table 2. The k-ranges used in the Fourier transform were 2.5−9.5 Å^{-1} for $Al_{0.75}Sc_{0.25}N$ and $Al_{0.7}Sc_{0.3}N$ and 3−11 Å^{-1} for ScN. The r-ranges used were 1.0−2.205, 1.0−2.607, and 1.0−3.229 Å for $Al_{0.75}Sc_{0.25}N$, $Al_{0.7}Sc_{0.3}N$, and ScN, respectively.

https://doi.org/10.1021/acsaelm.3c01390
ACS Appl. Electron. Mater. 2024, 6, 853−861

Table 2. EXAFS Fitting Results for $(Al_{0.75}Sc_{25})N$, $(Al_{0.70}Sc_{30})N$, ScN Powder, $(Al_{0.75}Y_{25})N$, and Y Foil[a,b]

sample	path	CN	S_0^2	R (Å)	σ^2 (Å^2)	ΔE_0 (eV)
$Al_{0.75}Sc_{0.25}N$	Sc−N	4	0.81 ± 0.27	2.11 ± 0.03	0.005 ± 0.005	1.0 ± 3.4
$Al_{0.70}Sc_{0.30}N$	Sc−N	4	0.69 ± 0.17	2.12 ± 0.02	0.004 ± 0.004	−0.5 ± 2.6
ScN	Sc−N	6	0.34 ± 0.05	2.27 ± 0.03	0.001 ± 0.003	2.4 ± 3.9
	Sc−Sc	12	0.34 ± 0.05	3.19 ± 0.01	0.001 ± 0.001	−3.0 ± 1.5
$Al_{0.75}Y_{0.25}N$	Y−N	3.7 ± 1.3	0.82	2.24 ± 0.03	0.000 ± 0.006	−4.2 ± 3.3
Y foil	Y−Y	12	0.82 ± 0.16	3.61 ± 0.01	0.014 ± 0.002	−0.8 ± 0.9
AlN[25]	Al−N	4		1.92 ± 0.01		

[a]CN is the coordination number (i.e., number of nearest neighbors at distance R per absorbing atom); R is the first near neighbor distance; σ^2 is the mean squared relative bond disorder (also referred to as the EXAFS Debye−Waller factor); ΔE_0 is the correction in the photoelectron energy origin, and S_0^2 is the amplitude reduction factor. [b]Reference to structural AlN data from the literature.[25]

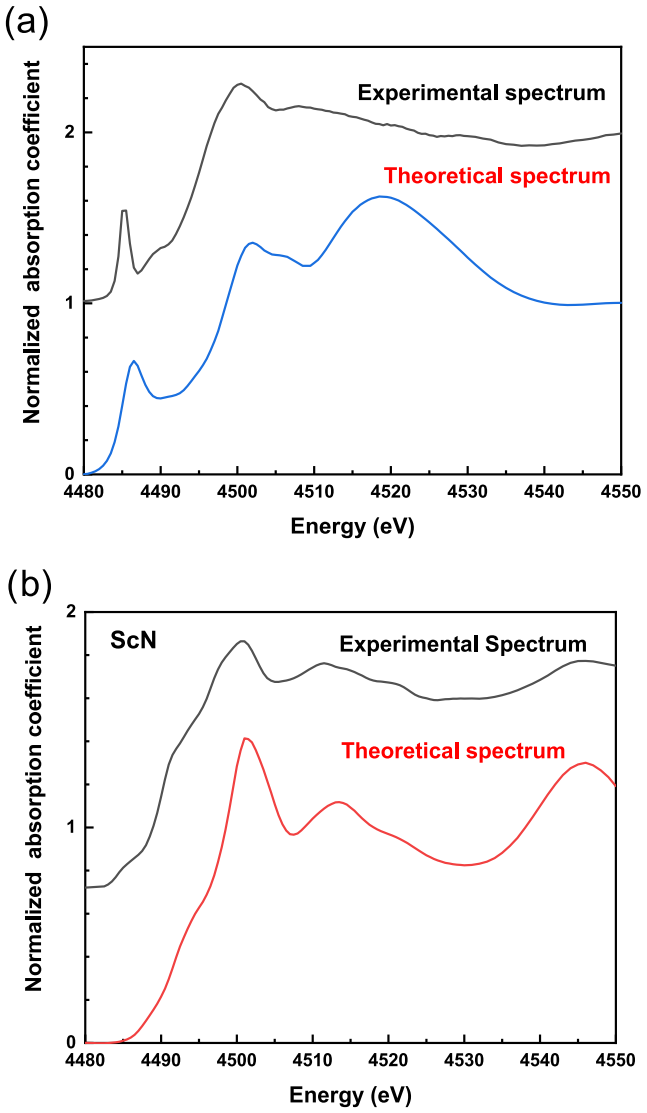

Figure 7. (a) Measured (black curve) and calculated (blue curve) XANES spectra of a $Al_{0.75}Sc_{0.25}N$ thin film; (b) measured (black curve) and calculated (red curve) XANES spectra of ScN powder.

peak is weaker for $Al_{0.70}Sc_{0.30}N$ than for $Al_{0.75}Sc_{0.25}N$. Possible explanations for this change include: (i) a homogeneous model for $x = 0.30$, in which Sc ions are all located in a relatively more symmetric environment, averaged over time, than the Al ions; or (ii) assuming a heterogeneous model for $x = 0.30$, in which some (unknown) fraction of the Sc ions reside in a symmetric local environment and the remainder do not. Due to the ensemble-average nature of X-ray absorption spectroscopy,[23] it is not possible to reliably distinguish between these two models on the basis of the XANES data alone.

Examining the EXAFS spectra (Figure 5a) demonstrates that the Fourier transform (Figure 5b) magnitudes of k^2-weighted EXAFS spectra for the ScN powder reveal a strong second shell peak near 2.61 Å and a weaker first shell peak in r-space. For $Al_{1-x}Sc_xN$, $x = 0.25$, 0.30, the first shell peak is prominent, and the peak position is shifted to smaller spacings relative to those observed for ScN. Models for each sample were calculated using the Demeter data analysis package with FEFF6 code fit to the EXAFS data (Figure 6a−c). As is evident in the XANES spectrum, the coordination number of Sc would be expected to be 4. Analysis of Sc K edge EXAFS could not independently verify the 4-coordinated Sc environment model due to the relatively large error bars in the coordination numbers (relative error of ca. 25%). Thus, for confirming the value of CN = 4 expected for Sc, we examined the mean value of the passive electron reduction factor, S_0^2,[24] that was allowed to vary for each material, assuming a fixed number of nearest neighbors (4), and obtained from the fit of EXAFS theory to the data. The fitting results for $Al_{0.75}Sc_{0.25}N$, $Al_{0.70}Sc_{0.30}N$, and ScN are given in Table 2. As expected, the S_0^2 values for the thin films were found to lie between 0.7 and 1.0, thereby supporting the model we have used. However, the ScN reference spectrum measured on a powder sample exhibited strong self-absorption. As such, the amplitude factor obtained was smaller than expected (Table 2), but the interatomic distances, not perturbed by the self-absorption effect, are very informative for choosing the proper model for Sc placement in AlN.

The results presented in Table 2 demonstrate that the first shell Sc−N distances in tetrahedrally coordinated $Al_{0.75}Sc_{0.25}N$ and $Al_{0.70}Sc_{0.30}N$ are similar, 2.11 ± 0.03 and 2.12 ± 0.02 Å respectively, whereas the Sc−N distance in octahedrally coordinated ScN is larger, 2.27 ± 0.03 Å. Hence, 0.16 Å shortening occurs when the scandium ion local environment changes from octahedral to tetrahedral configuration. The second shell, Sc−Sc distance in ScN, was found to be 3.19 ± 0.01 Å. By subtracting the $N^{3-}_{CN=4}$ Shannon crystal radius (1.32 Å)[9] from the Sc−N distance in AlScN, the crystal radius of $Sc^{3+}_{CN=4}$ species of 0.79 ± 0.02 Å may be estimated. The same calculation can be made for $Al^{3+}_{CN=4}$ using the Al−N distance from the literature (1.901 Å).[25] This results in a crystal radius for $Al^{3+}_{CN=4}$ of 0.58 Å, i.e., only 5 pm larger than the value reported by ref 9. Consequently, we may assert that the difference between the crystal radii of the solute and solvent atoms for $Al_{0.75}Sc_{0.25}N$ and $Al_{0.70}Sc_{0.30}N$ is ∼36%. We have performed theoretical modeling of the Sc K-edge XANES spectra using FEFF9 code,[26] calibrating the input parameters

https://doi.org/10.1021/acsaelm.3c01390
ACS Appl. Electron. Mater. 2024, 6, 853−861

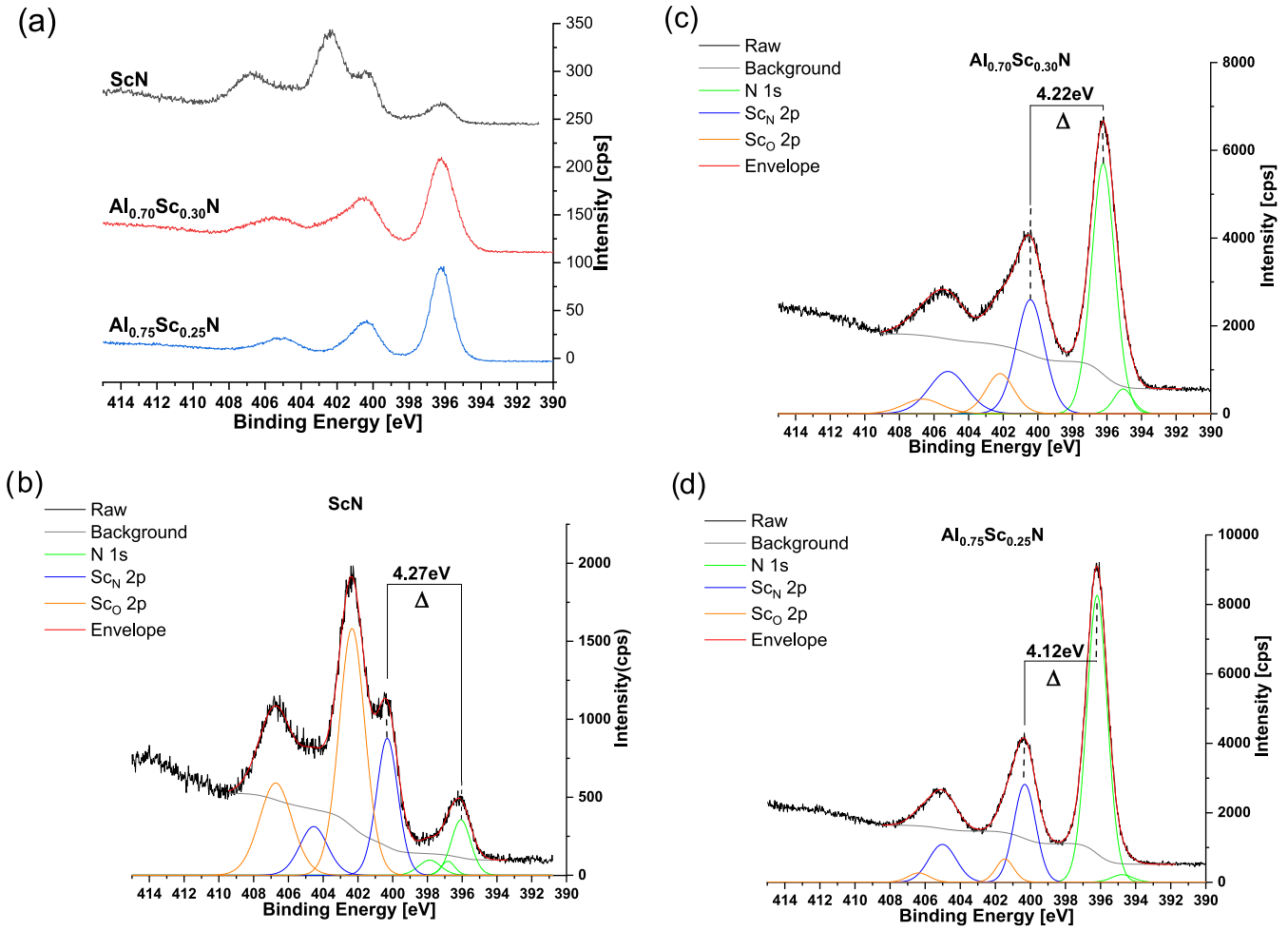

Figure 8. (a) X-ray photoelectron spectra of the binding energy of N 1s and Sc 2p electrons in $Al_{0.75}Sc_{0.25}N$ (blue trace) and $Al_{0.7}Sc_{0.3}N$ (red trace) thin films and ScN (black trace) powder samples. Profile fitting was performed for each of the three samples: (b) ScN; (c) $Al_{0.7}Sc_{0.3}N$; (d) $Al_{0.75}Sc_{0.25}N$ in order to estimate the amplitude of the observed increase in Δ with increase in Sc doping in the wurtzite lattice.

using the agreement between the experimental and theoretical ScN spectra (Figure 7a). The same parameters were used to obtain simulated XANES spectra of a structure of $Al_{0.75}Sc_{0.25}N$ (Figure 7b). The resulting simulation displays a spectrum with the same prominent pre-edge peak as observed in the experiment.

X-ray Photoelectron Spectroscopy (XPS) of Sc-Doped Aluminum Nitride. Complementary information was obtained from XPS analysis. This surface-sensitive technique, typically probing to a depth ≤15 nm below the film surface, revealed significant surface oxidation, accompanied by surface Sc-depletion. Therefore, for any quantitative analysis of fine details in the Sc oxidation states, we relied on (1) comparison to a reference ScN sample and (2) stepwise Ar-ion etching that enabled gradual removal of surface species, including close inspection of beam-induced artifacts. Figure 8a presents the N 1s + Sc 2p spectral window, recorded from a reference ScN powder and from $Al_{1-x}Sc_xN$ (x = 0.25 and 0.30) films after etching the surface by Ar-ions. Notably, the reference sample exhibits three nitrogen signals (green curves in Figure 8b) and two Sc doublets, attributed to ScN (blue components) as well as to Sc_2O_3 (orange components). Both Sc doublets and the main N 1s signal provide useful references for the ternary thin films. As shown in Figure 8c,d, the etched films consist of a single N 1s signal and two Sc doublets. Similarity to the reference spectrum in Figure 8b is apparent. Details of the XPS-derived surface stoichiometry are provided in the Supporting Information file (Section S3 and Table S4). Notably, the energy difference, Δ, between the N 1s peak and the ScN-related doublet reveals small variations for the different samples, as indicated in Figure 8. These variations propose a slightly more electron-rich environment for Sc at low-x values, ≈100 meV in magnitude (compare Figure 8c,d). This latter observation does, of course, suffer from the possible presence of unknown potential effects on the nitrogen signal and, therefore, must be considered only as a secondary support for the XAS result.

Two comments should be added in this respect. First, the XPS of nonetched surfaces (data not shown) are in agreement with the Sc binding energy behavior as described above. Second, for a ≈100 meV difference in Δ$v$alues between (nominally) x = 0.25 and 0.30 (Figure 8c,d), the actual difference may be larger: coexistence of two environments should be analyzed as two superimposed signals. Nevertheless, the XPS data are consistent with the presence of two Sc−N local environments: CN = 4, dictated by the AlN host, dominant at low Sc concentrations, and CN = 6 environment, which increases as the Sc concentration increases.

Our suggestion that at 30 mol % Sc doping in sputtered AlN thin films, a small fraction of the Sc^{3+} ions are coordinated by 6

https://doi.org/10.1021/acsaelm.3c01390
ACS Appl. Electron. Mater. 2024, 6, 853−861

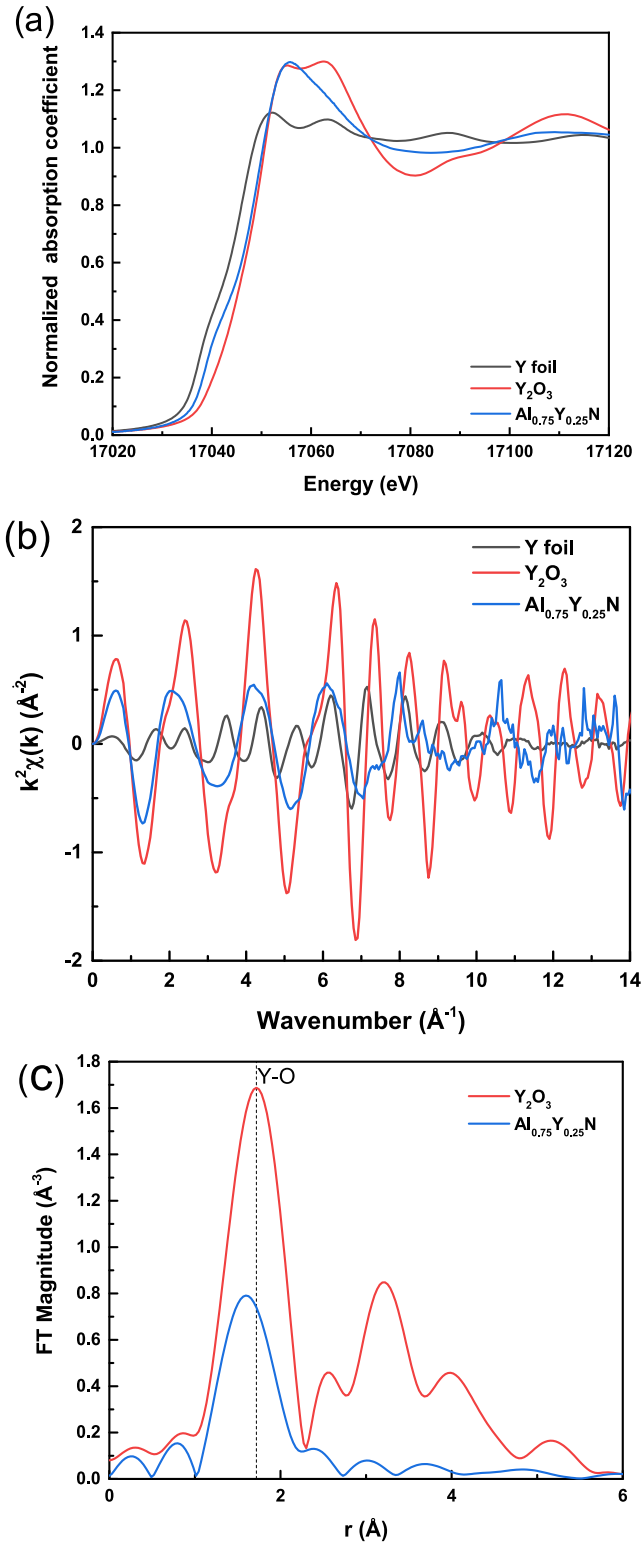

Figure 9. (a) Normalized Y K-edge XANES spectrum of $Al_{0.75}Y_{0.25}N$. For comparison, the spectra of Y foil and Y_2O_3 are included. (b) The k^2-weighted EXAFS spectra of $Al_{0.75}Y_{0.25}N$ thin film, Y_2O_3 powder, and Y foil. (c) Fourier transform magnitude of the k^2 -weighted $\chi(k)$ spectra. The k range for the Fourier transformation is 2−7.5 Å^{-1}.

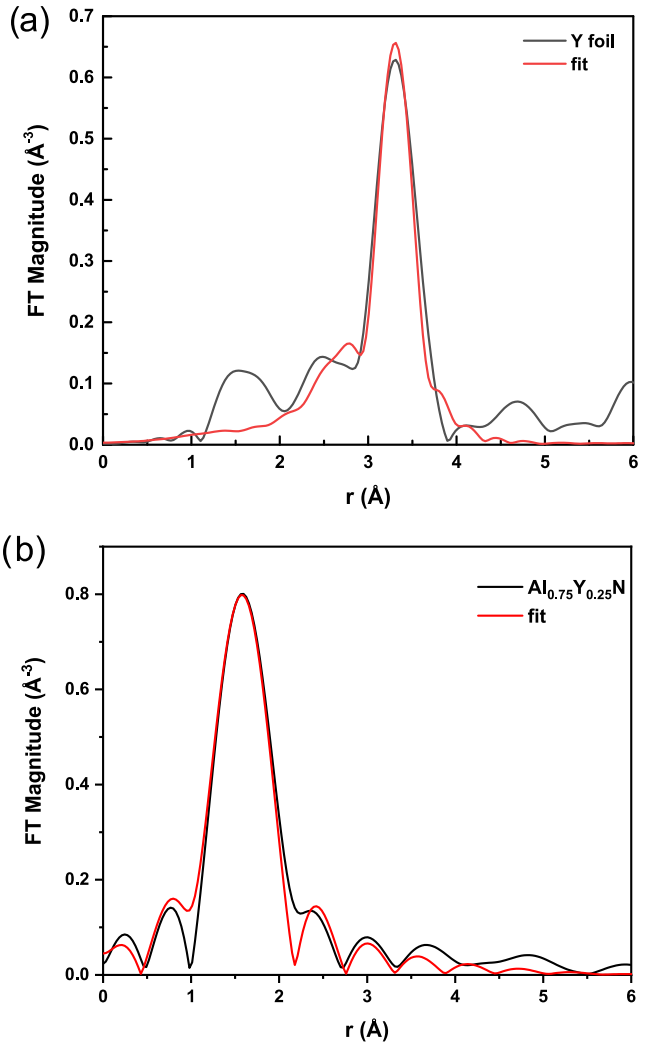

Figure 10. Measured (black curve) and fitted (red curve) Fourier transform magnitude of the k^2-weighted EXAFS spectrum for (a) Y foil. The k range for the Fourier transform is 2−12 Å^{-1}. The r range is 2.6−4 Å; (b) $Al_{0.75}Y_{0.25}N$ film. The k range for the Fourier transform is 2−7.5 Å^{-1}. The r range is 1.3−3.3 Å.

rather than by 4 N atoms does not contradict the well-documented increase in the piezoelectric strain coefficient d_{33}. Rather, wurtzite lattice destabilization, brought about by the attempt to incorporate a large cation that prefers coordination number (CN) = 6, can indeed explain this effect. A destabilized, mechanically softer lattice is more readily deformed in the presence of an applied stress or electric field. As reviewed by Ambacher et al.,[27] the stiffness coefficient $C_{33}(x)$ decreases due to the alloying of wurtzite-AlN with rock-salt-ScN, but at the same time, the piezoelectric coefficient $d_{33}(x)$ increases very sharply up to the miscibility limit. This finding is similar to the mechanism suggested for the case of the morphotropic phase boundary (MPB) in solid solutions of $PbZrO_3$−$PbTiO_3$ (PZT),[28] although, unlike (Al, Sc)N, this system displays full miscibility. In PZT, the coexistence of different structures, even if nonpiezoelectric,[29] increases the piezoelectric response in the vicinity of the MPB because it destabilizes the lattice. So, the more compliant the lattice, the larger the response.

X-ray Absorption Fine Structure (XAFS) of Y-Doped Aluminum Nitride. K-edge XANES spectra of Y foil, Y_2O_3 powder, and $Al_{0.75}Y_{0.25}N$ thin film samples are shown in Figure 9a. Although present, the pre-edge peak, indicative of local asymmetry for Y in the thin film, is substantially weaker than that observed for the Sc-doped samples. This might be

https://doi.org/10.1021/acsaelm.3c01390
ACS Appl. Electron. Mater. 2024, 6, 853−861

anticipated for a 4d atom, in comparison to a 3d atom, due to broadening effects.[30] The shape of the Y K-edge XANES spectrum of $Al_{0.75}Y_{0.25}N$ differs from that of double fluorite Y_2O_3 (Figure 9), indicating that the local environment of Y^{3+} in $Al_{0.75}Y_{0.25}N$ is unlike that in Y_2O_3, as expected. In comparison to Y_2O_3, the intensity of the first shell peak obtained by FT of the k^2 weighted absorption spectrum (Figure 9b) is much weaker and the position of the peak is shifted to smaller r values in $Al_{0.75}Y_{0.25}N$ (Figure 9c). From this, we conclude that the mean coordination number in $Al_{0.75}Y_{0.25}N$ is smaller than 6. Y foil measured on the same beamline was analyzed to obtain the passive electron reduction factor (S_0^2) of Y. The value for S_0^2 (0.82) was used in fitting the $Al_{0.75}Y_{0.25}N$ spectrum (Figure 10). The coordination number (CN), which was allowed to vary for Y in $Al_{0.75}Y_{0.25}N$, is 3.7 ± 1.3. The Y−N bond length in $Al_{0.75}Y_{0.25}N$ was found to be 2.24 ± 0.03 Å, while the literature value (ICSD #37413) for YN bond length in the rock-salt structure, octahedral coordination, is 2.438 Å. Accordingly, the $Y^{3+}_{CN=4}$ crystal radius is estimated to be 0.92 ± 0.01 Å compared to 1.118 Å for $Y^{3+}_{CN=6}$[9]. Consequently, the difference between the crystal radius of the solute and solvent atoms for $Al_{0.75}Y_{0.25}N$ is ∼58%.

CONCLUSIONS

In summary, the local structure and chemical environment of Sc and Y in predominantly ⟨002⟩ textured, $Al_{1-x}Do_xN$ (Do = Sc, x = 0.25, 0.30 or Y, x = 0.25) sputtered thin films with wurtzite symmetry were investigated using XRD, XAS and XPS techniques. We present evidence from X-ray absorption spectroscopy that at the relatively low doping levels investigated, both Sc^{3+} and Y^{3+} ions substitute for Al^{3+} in the wurtzite lattice, thereby assuming a coordination number of four. On this basis, the effective size of the ion species in their respective coordination state could be calculated. Introducing dopants causes an increase in lattice strain, which is manifested macroscopically as increased in-plane compressive stress, particularly in the case of Y-doped AlN. By modeling the scandium local environment, EXAFS is able to suggest that a small fraction of the dopant ions experience an increase in coordination number from 4 to 6 when the dopant concentration is increased from 25 to 30 mol %. In other words, a small population of scandium ions appears to experience a change from tetrahedral to octahedral coordination at a dopant concentration significantly lower than that reported for the global wurtzite to rock-salt phase transition (42 mol % Sc[13,31,32]). In the ScN rock-salt lattice, Sc ions are all octahedrally coordinated and are in a centrosymmetric local environment. Our proposed heterogeneous model for the 30 mol % sample, based also on the weakening of the pre-edge peak in the XANES spectra, would therefore support some partitioning of Sc ions into rock-salt-like ScN_x clusters within the wurtzite matrix. XPS provides supporting evidence for this observation. Given that the Sc ions are responsible for an increase in piezoelectric response observed for doped AlN, it remains uncertain whether tetrahedrally coordinated or octahedrally coordinated Sc ions (or both) are responsible.

ASSOCIATED CONTENT

Supporting Information

The Supporting Information is available free of charge at https://pubs.acs.org/doi/10.1021/acsaelm.3c01390.

Section S1: expanded 2θ range of the XRD pattern for the $Al_{0.75}Y_{0.25}N$ sample; Section S2: EDS analysis of the (Al,Sc)N films and (Al,Y)N film; Section S3: XPS analysis of (Al, Sc)N films (PDF)

AUTHOR INFORMATION

Corresponding Authors

Igor Lubomirsky − *Department of Molecular Chemistry and Materials Science, Weizmann Institute of Science, Rehovot 7610001, Israel;* orcid.org/0000-0002-2359-2059; Email: igor.lubomirsky@weizmann.ac.il

Anatoly I. Frenkel − *Department of Materials Science and Chemical Engineering, Stony Brook University, Stony Brook, New York 11794, United States;* orcid.org/0000-0002-5451-1207; Email: anatoly.frenkel@stonybrook.edu

David Ehre − *Department of Molecular Chemistry and Materials Science, Weizmann Institute of Science, Rehovot 7610001, Israel;* orcid.org/0000-0002-5522-8059; Email: david.ehre@weizmann.ac.il

Authors

Asaf Cohen − *Department of Molecular Chemistry and Materials Science, Weizmann Institute of Science, Rehovot 7610001, Israel*

Junying Li − *Department of Materials Science and Chemical Engineering, Stony Brook University, Stony Brook, New York 11794, United States*

Hagai Cohen − *Department of Chemical Research Support, Weizmann Institute of Science, Rehovot 7610001, Israel;* orcid.org/0000-0001-8488-0727

Ifat Kaplan-Ashiri − *Department of Chemical Research Support, Weizmann Institute of Science, Rehovot 7610001, Israel*

Sergey Khodorov − *Department of Molecular Chemistry and Materials Science, Weizmann Institute of Science, Rehovot 7610001, Israel*

Ellen J. Wachtel − *Department of Molecular Chemistry and Materials Science, Weizmann Institute of Science, Rehovot 7610001, Israel*

Complete contact information is available at: https://pubs.acs.org/10.1021/acsaelm.3c01390

Author Contributions

The manuscript was written with contributions from all authors. All authors have approved the final version.

Funding

X-ray absorption spectroscopy studies and data analysis by A.I.F. were supported by NSF Grant number DMR-2312690. I.L. acknowledges the BSF program grant 2022786 for his contribution to the XAS studies. These grants are the two parts of the NSF-BSF grant awarded to A.I.F. and I.L., respectively. This research used beamlines 7-BM and 8-BM of the National Synchrotron Light Source II (NSLS-II), a U.S. DOE Office of Science User Facility operated for the DOE Office of Science by Brookhaven National Laboratory under contract no. DE-SC0012704. The authors acknowledge support by the Synchrotron Catalysis Consortium funded by the US Department of Energy, Office of Science, Office of Basic Energy Sciences, Grant No. DE-SC0012335. A.I.F. acknowledges support by a Weston Visiting Professorship during his stay at the Weizmann Institute of Science. This work is made possible

in part by the historic generosity of the Harold Perlman Family.

Notes

The authors declare no competing financial interest.

REFERENCES

(1) Aigner, R.; Kaitila, J.; Ella, J.; Elbrecht, L.; Nessler, W.; Handtmann, M.; Herzog, T. R.; Marksteiner, S. Bulk-Acoustic-Wave Filters: Performance Optimization and Volume Manufacturing. In *2003 IEEE MTT-S International Microwave Symposium Digest*, Vols 1−3, 2001−2004; IEEE, 2003.

(2) Elfrink, R.; Kamel, T. M.; Goedbloed, M.; Matova, S.; Hohlfeld, D.; van Andel, Y.; van Schaijk, R. Vibration energy harvesting with aluminum nitride-based piezoelectric devices. *J. Micromech. Microeng.* **2009**, *19* (9), No. 094005.

(3) Mayrhofer, P. M.; Riedl, H.; Euchner, H.; Stoger-Pollach, M.; Mayrhofer, P. H.; Bittner, A.; Schmid, U. Microstructure and piezoelectric response of $Y_xAl_{1-x}N$ thin films. *Acta Mater.* **2015**, *100*, 81−89.

(4) Uehara, M.; Shigemoto, H.; Fujio, Y.; Nagase, T.; Aida, Y.; Umeda, K.; Akiyama, M. Giant increase in piezoelectric coefficient of AlN by Mg-Nb simultaneous addition and multiple chemical states of Nb. *Appl. Phys. Lett.* **2017**, *111* (11), No. 112901.

(5) Sandu, C. S.; Parsapour, F.; Mertin, S.; Pashchenko, V.; Matloub, R.; LaGrange, T.; Heinz, B.; Muralt, P. Abnormal Grain Growth in AlScN Thin Films Induced by Complexion Formation at Crystallite Interfaces. *Phys. Status Solidi A* **2019**, *216* (2), No. 1800569.

(6) Akiyama, M.; Kano, K.; Teshigahara, A. Influence of growth temperature and scandium concentration on piezoelectric response of scandium aluminum nitride alloy thin films. *Appl. Phys. Lett.* **2009**, *95* (16), No. 162107.

(7) Kanouni, F.; Amara, S.; Laidoudi, F. Thin Film Bulk Acoustic Resonators based on c-Axis Tilted Yttrium-doped AlN for Viscosity Sensors. In *19th International Multi-Conference on Systems, Signals & Devices (SSD'22)*; IEEE, 2022.

(8) Schuster, J. C.; Bauer, J. The Ternary-Systems Sc-Al-N and Y-Al-N. *J. Less-Common Met.* **1985**, *109* (2), 345−350.

(9) Shannon, R. D. Revised effective ionic radii and systematic studies of interatomic distances in halides and chalcogenides. *Acta Crystallogr., Sect. A: Cryst. Phys., Diffr., Theor. Gen. Crystallogr.* **1976**, *32* (5), 751−767.

(10) Cheng, H.; Sun, Y.; Hing, P. The influence of deposition conditions on structure and morphology of aluminum nitride films deposited by radio frequency reactive sputtering. *Thin Solid Films* **2003**, *434* (1−2), 112−120.

(11) Akiyama, M.; Nagao, K.; Ueno, N.; Tateyama, H.; Yamada, T. Influence of metal electrodes on crystal orientation of aluminum nitride thin films. *Vacuum* **2004**, *74* (3−4), 699−703.

(12) Artieda, A.; Barbieri, M.; Sandu, C. S.; Muralt, P. Effect of substrate roughness on c-oriented AlN thin films. *J. Appl. Phys.* **2009**, *105* (2), No. 024504.

(13) Akiyama, M.; Kamohara, T.; Kano, K.; Teshigahara, A.; Takeuchi, Y.; Kawahara, N. Enhancement of Piezoelectric Response in Scandium Aluminum Nitride Alloy Thin Films Prepared by Dual Reactive Cosputtering. *Adv. Mater.* **2009**, *21* (5), 593−596.

(14) Laidoudi, F.; Kanouni, F.; Assali, A.; Caliendo, C.; Amara, S.; Nezzari, H.; Boubenider, F. Thickness shear SMR resonator based on yttrium-doped AlN for high sensitive liquid sensors. *Sens. Actuators, A* **2022**, *333*, No. 113238.

(15) Žukauskaitė, A.; Tholander, C.; Palisaitis, J.; Persson, P. O. Å.; Darakchieva, V.; Sedrine, N. B.; Tasnádi, F.; Alling, B.; Birch, J.; Hultman, L. $Y_xAl_{1-x}N$ thin films. *J. Phys. D: Appl. Phys.* **2012**, *45* (42), No. 422001.

(16) Fryzuk, M. D.; Giesbrecht, G.; Rettig, S. J. Synthesis and Characterization of the Five-Coordinate Scandium Dialkyl Complexes $ScR_2[N(SiMe_2CH_2PPr^i_2)_2]$ (R = Me, Et, CH_2SiMe_3). *Organometallics* **1996**, *15* (15), 3329−3336.

(17) Cohen, A.; Cohen, H.; Cohen, S. R.; Khodorov, S.; Feldman, Y.; Kossoy, A.; Kaplan-Ashiri, I.; Frenkel, A.; Wachtel, E.; Lubomirsky, I.; Ehre, D. C-Axis Textured, 2−3 μm Thick $Al_{0.75}Sc_{0.25}N$ Films Grown on Chemically Formed TiN/Ti Seeding Layers for MEMS Applications. *Sensors* **2022**, *22* (18), No. 7041, DOI: 10.3390/s22187041.

(18) Freund, L. B.; Floro, J.; Chason, E. Extensions of the Stoney formula for substrate curvature to configurations with thin substrates or large deformations. *Appl. Phys. Lett.* **1999**, *74* (14), 1987−1989.

(19) Vedrinskii, R. V.; Kraizman, V. L.; Novakovich, A. A.; Demekhin, P. V.; Urazhdin, S. V. Pre-edge fine structure of the 3d atom K x-ray absorption spectra and quantitative atomic structure determinations for ferroelectric perovskite structure crystals. *J. Phys.: Condens. Matter* **1998**, *10* (42), 9561−9580.

(20) Farges, F.; Brown, G. E.; Rehr, J. J. Ti K-edge XANES studies of Ti coordination and disorder in oxide compounds: Comparison between theory and experiment. *Phys. Rev. B* **1997**, *56* (4), 1809−1819.

(21) Frenkel, A. I.; Ehre, D.; Lyahovitskaya, V.; Kanner, L.; Wachtel, E.; Lubomirsky, I. Origin of polarity in amorphous SrTiO3. *Phys. Rev. Lett.* **2007**, *99* (21), No. 215502.

(22) Frenkel, A. I.; Feldman, Y.; Lyahovitskaya, V.; Wachtel, E.; Lubomirsky, I. Microscopic origin of polarity in quasiamorphous BaTiO3. *Phys. Rev. B* **2005**, *71* (2), No. 024116.

(23) Routh, P. K.; Marcella, N.; Frenkel, A. I. Speciation of Nanocatalysts Using X-ray Absorption Spectroscopy Assisted by Machine Learning. *J. Phys. Chem. C* **2023**, *127*, 5653−5662.

(24) Roy, M.; Gurman, S.; Van Dorssen, G. The amplitude reduction factor in EXAFS. *J. Phys. IV* **1997**, *7* (C2), C2−151−C2−152, DOI: 10.1051/jp4/1997146.

(25) Aslam, M. Z.; Jeoti, V.; Karuppanan, S.; Malik, A. F.; Iqbal, A. FEM Analysis of Sezawa Mode SAW Sensor for VOC Based on CMOS Compatible $AlN/SiO_2/Si$ Multilayer Structure. *Sensors* **2018**, *18* (6), No. 1687, DOI: 10.3390/s18061687.

(26) Rehr, J. J.; Kas, J. J.; Vila, F. D.; Prange, M. P.; Jorissen, K. Parameter-free calculations of X-ray spectra with FEFF9. *Phys. Chem. Chem. Phys.* **2010**, *12* (21), 5503−5513.

(27) Ambacher, O.; Mihalic, S.; Yassine, M.; Yassine, A.; Afshar, N.; Christian, B. Review: Structural, elastic, and thermodynamic properties of cubic and hexagonal $Sc_xAl_{1-x}N$ crystals. *J. Appl. Phys.* **2023**, *134* (16), No. 112103.

(28) Damjanovic, D. Ferroelectric, dielectric and piezoelectric properties of ferroelectric thin films and ceramics. *Rep. Prog. Phys.* **1998**, *61* (9), No. 1267, DOI: 10.1088/0034-4885/61/9/002.

(29) Zhang, N.; Yokota, H.; Glazer, A. M.; Ren, Z.; Keen, D. A.; Keeble, D. S.; Thomas, P. A.; Ye, Z. G. The missing boundary in the phase diagram of $PbZr_{1-x}Ti_xO_3$. *Nat. Commun.* **2014**, *5* (1), No. 5231.

(30) Yamamoto, T. Assignment of pre-edge peaks in K-edge X-ray absorption spectra of 3d transition metal compounds: electric dipole or quadrupole? *X-Ray Spectrom.* **2008**, *37* (6), 572−584.

(31) Deng, R.; Evans, S. R.; Gall, D. Bandgap in $Al_{1-x}Sc_xN$. *Appl. Phys. Lett.* **2013**, *102* (11), No. 112103.

(32) Mertin, S.; Heinz, B.; Rattunde, O.; Christmann, G.; Dubois, M.-A.; Nicolay, S.; Muralt, P. Piezoelectric and structural properties of c-axis textured aluminium scandium nitride thin films up to high scandium content. *Surf. Coat. Technol.* **2018**, *343*, 2−6.

https://doi.org/10.1021/acsaelm.3c01390
ACS Appl. Electron. Mater. 2024, 6, 853−861